Local multiquadric approximation for solving boundary value problems

*C. K. Lee[1], X. Liu, and S. C. Fan

School of Civil and Environmental Engineering
Nanyang Technological University
Nanyang Avenue
Singapore 639798

*Emails: [1]ccklee@ntu.edu.sg

Preprint version of the paper in Computational Mechanics, Vol. 30, Issue 5-6, pp 396-409 (2003)

Summary

This paper presents a truly meshless approximation strategy for solving partial differential equations based on the local multiquadric (LMQ) and the local inverse multiquadric (LIMQ) approximations. It is different from the traditional global multiquadric (GMQ) approximation in such a way that it is a pure local procedure. In constructing the approximation function, the only geometrical data needed is the local configuration of nodes fallen within its influence domain. Besides this distinct characteristic of localization, in the context of meshless-typed approximation strategies, other major advantages of the present strategy include: (i) the existence of the shape functions is guaranteed provided that all the nodal points within an influence domain are distinct; (ii) the constructed shape functions strictly satisfy the Kronecker delta condition; (iii) the approximation is stable and insensitive to the free parameter embedded in the formulation and; (iv) the computational cost is modest and the matrix operations require only inversion of matrices of small size which is equal to the number of nodes inside the influence domain. Based on the present LMQ and LIMQ approximations, a collocation procedure is developed for solutions of 1D and 2D boundary value problems. Numerical results indicate that the present LMQ and LIMQ approximations are more stable than their global counterparts. In addition, it demonstrates that both approximation strategies are highly efficient and able to yield accurate solutions regardless of the chosen value for the free parameter.

KEYWORDS: local multiquadric approximation, local inverse multiquadric approximation, radical base functions, meshless method, collocation procedure

---

[1]Correspondence author

1. Introduction

Recently, the so-called "meshless methods" emerged as a potential alternative for solutions in computational mechanics and a variety of approaches named after "meshless" have appeared. They can be categorised into two main groups, with respect to their approximation techniques:

i) Methods based on the Galerkin integration technique

For those methods grouped under this category, their final numerical equations are generated by substituting the approximation functions into an (Galerkin) integration equation. It includes the element-free Galerkin method [1,2], the reproducing kernel particle method [3,4], the *h*-*p*- cloud method [5], the partition-of-unity method [6], the meshless local Petrov-Galerkin method [7] and the point interpolation method [8].

ii) Methods based on point collocation technique

This group embraces methods which base on kinds of collocation technique to generate the final numerical equations. Examples include the finite point [9,10] and the finite cloud [11] method, the multiquadric (MQ) and other methods in which the formulations are based on the radial basis functions (RBF) [12-18].

In the above-mentioned meshless methods, the way of constructing their approximate field functions is one of the most important features that affect their performance, stability and efficiency. A wealth of novel way of the construction can be found in literature. The most popular approaches include the moving-least-square method (MLSM) [1,2], the kernel integration approximation [3,4], the point interpolation method [8], the natural neighbour interpolation [19] and various MQ-RBF approaches. Among them, the MLSM is frequently used and has acquired a great success. However, the MLSM also suffers some shortcomings such as lack of interpolating property and its high computational cost.

The MQ-RBF approach has undergone intensive research and enjoyed considerable success as a technique for interpolating multivariate data and functions [12-18]. In 1982, Franke [13] wrote a review article. In it, he evaluated thoroughly various interpolation methods for scattered data. Among the methods evaluated, Hardy's MQ [12] was ranked the best in accuracy. Kansa [14] employed different MQ-RBFs in solving different partial differential equations (PDEs). Hon et al. [15] further extended the MQ-RBFs to obtain numerical solutions for various PDEs. Golberg and Chen [16-17] proposed an improved MQ formulation. In it, some important features with respect to the development of MQ-RBFs method were highlighted as follows.

a) The MQ-RBF is a truly meshless approach.

b) It is profoundly suitable for constructing mathematical models over a set of scattered data.

c) The convergence rate is of the order $O(h^{ND+1})$. In it, h denotes the spacing between collocation points and ND denotes the spatial dimension. This property enhances its applicability in solving higher-dimensional problems.

Nevertheless, the MQ formulation has a free shape parameter 'c' embedded in its procedure. The value of 'c' has a great influence on the accuracy of the solution. To choose an optimal shape parameter 'c' is a tricky issue and it remains to be an open question and no mathematical theory has been put forward to determine the optimal 'c' value. Besides, the computational cost of those MQ methods is high since many MQ formulations employ the global interpolation approach and resulting in fully populated coefficient matrices. Furthermore, those fully populated matrices tend to become progressively more ill-conditioned as the number of collocation points increases. Against this background, this paper presents two new strategies, namely the local MQ (LMQ) and the local inverse MQ (LIMQ) strategies, which formulations result in well-conditioned and banded coefficient matrices.

Next section will present the formulation of LMQ and the LIMQ approximations. It is then followed by the description of the collocation technique used in this study. Subsequently, the performance and efficiency of the present strategies are illustrated through solutions of some elliptic PDEs in 1D or 2D. Finally, conclusions are drawn on the effectiveness and stability of the present methods.

2. Local multiquadric and local inverse miltiquadric approximations

By using the local multiquadric approximation strategy, $\hat{u}(\mathbf{x})$, the approximation of a function $u(\mathbf{x})$ at an arbitrary point $\mathbf{x}$ can be written as a linear combination of n multiquadric functions in the following form:

$$u(\mathbf{x}) \approx \hat{u}(\mathbf{x}) = \sum_{i=1}^{n} a_i \phi(\|\mathbf{r} - \mathbf{r}_i\|, c) \qquad (1)$$

In Eqn. 1, n is the number of nodal points fallen within the influence domain $\Omega_{\mathbf{x}}$ (or *cover*) of $\mathbf{x}$ (Fig. 1). c denotes a free parameter and a_i are coefficients to be determined. ϕ_i are the *multiquardic functions* defined as

$$\phi(\|\mathbf{r} - \mathbf{r}_i\|, c) = \sqrt{\|\mathbf{r} - \mathbf{r}_i\|^2 + c^2} \qquad (2)$$

where $\|\mathbf{r} - \mathbf{r}_i\|$ denotes the distance between $\mathbf{x}$ and the i^{th} nodal point $\mathbf{x}_i$.

By using the local inverse multiquadrics (LIMQ) technique, u(**x**) can be written as

$$\hat{u}(\mathbf{x}) = \sum_{i=1}^{n} \frac{a_i}{\phi(\|\mathbf{r} - \mathbf{r}_i\|, c)} \tag{3}$$

by replacing $\phi(\|\mathbf{r} - \mathbf{r}_i\|, c)$ in Eqn. 1 by $\dfrac{1}{\phi(\|\mathbf{r} - \mathbf{r}_i\|, c)}$.

To obtain the values of the coefficients a_i, one can first evaluate Eqn. 1 (or Eqn. 3) at all nodal points $\mathbf{x}_i$, i=1,...,n within the cover and obtain

$$\begin{aligned} \hat{u}(\mathbf{x}_i) &= \sum_{j=1}^{n} a_i \phi(\|\mathbf{r}_i - \mathbf{r}_j\|, c) \\ &= a_1 \phi(\|\mathbf{r}_i - \mathbf{r}_1\|, c) + a_2 \phi(\|\mathbf{r}_i - \mathbf{r}_2\|, c) + ... + a_n \phi(\|\mathbf{r}_i - \mathbf{r}_n\|, c) \end{aligned} \tag{4a}$$

Eqn. 4a can be represented in the compact matrix form

$$\hat{\mathbf{u}} = \mathbf{\Phi}_n \mathbf{a} \tag{4b}$$

in which

$$\hat{\mathbf{u}} = [\hat{u}(\mathbf{x}_1), \hat{u}(\mathbf{x}_2), ..., \hat{u}(\mathbf{x}_n)]^T \quad \text{and} \quad \mathbf{a} = [a_1, a_2, ..., a_n]^T \tag{5}$$

and $\mathbf{\Phi}_n$ is an n×n real symmetric coefficient matrix defined as

$$\mathbf{\Phi}_n = \begin{bmatrix} c & \phi(\|\mathbf{r}_1 - \mathbf{r}_2\|, c) & \cdot & \cdot & \phi(\|\mathbf{r}_1 - \mathbf{r}_n\|, c) \\ \phi(\|\mathbf{r}_1 - \mathbf{r}_2\|, c) & c & & & \phi(\|\mathbf{r}_2 - \mathbf{r}_n\|, c) \\ \cdot & & & \cdot & \cdot \\ \cdot & & & c & \cdot \\ \phi(\|\mathbf{r}_1 - \mathbf{r}_n\|, c) & \phi(\|\mathbf{r}_2 - \mathbf{r}_n\|, c) & \cdot & \cdot & c \end{bmatrix} \tag{6}$$

If one defines

$$\begin{aligned} \mathbf{\varphi}_n(\mathbf{r}) &= [\phi(\|\mathbf{r}_1 - \mathbf{r}\|, c) \quad \phi(\|\mathbf{r}_2 - \mathbf{r}\|, c) \quad \cdot \quad \cdot \quad \phi(\|\mathbf{r}_n - \mathbf{r}\|, c)]^T \\ &= [\phi(\|\mathbf{r} - \mathbf{r}_1\|, c) \quad \phi(\|\mathbf{r} - \mathbf{r}_2\|, c) \quad \cdot \quad \cdot \quad \phi(\|\mathbf{r} - \mathbf{r}_n\|, c)]^T \end{aligned} \tag{7}$$

then the approximation function $\hat{u}(\mathbf{x})$ (Eqn. 1) and the matrix $\mathbf{\Phi}_n$ can be expressed as

$$\hat{u}(\mathbf{x}) = \boldsymbol{\varphi}_n(\mathbf{r})^T \mathbf{a} \quad \text{and} \quad \boldsymbol{\Phi}_n = \left[\boldsymbol{\varphi}_n(\mathbf{r}_1) \quad \boldsymbol{\varphi}_n(\mathbf{r}_2) \quad \cdot \quad \cdot \quad \boldsymbol{\varphi}_n(\mathbf{r}_n)\right] = \begin{bmatrix} \boldsymbol{\varphi}_n(\mathbf{r}_1)^T \\ \boldsymbol{\varphi}_n(\mathbf{r}_2)^T \\ \cdot \\ \cdot \\ \boldsymbol{\varphi}_n(\mathbf{r}_n)^T \end{bmatrix} \tag{8}$$

It can be proved that the matrix $\boldsymbol{\Phi}_n$ is non-singular such that $(\boldsymbol{\Phi}_n)^{-1}$ exists. $(\boldsymbol{\Phi}_n)^{-1}$can always be computed provided that (i) c≠0 and (ii) all the nodal points inside the cover $\Omega_{\mathbf{x}}$ of **x** are distinct points. The proof is shown in the Appendix. Upon computing $(\boldsymbol{\Phi}_n)^{-1}$, the column vector **a** can be obtained by writing

$$\mathbf{a} = \left(\boldsymbol{\Phi}_n\right)^{-1} \hat{\mathbf{u}} \tag{9}$$

The approximation function, $\hat{u}(\mathbf{x})$ can now be expressed in terms of the nodal values, $\hat{\mathbf{u}}$. That is

$$\begin{aligned} \hat{u}(\mathbf{x}) &= \boldsymbol{\varphi}_n(r)^{\mathbf{T}} \left(\boldsymbol{\Phi}_n\right)^{-1} \hat{\mathbf{u}} \\ &= \boldsymbol{\Psi}_n(r)^{\mathbf{T}} \hat{\mathbf{u}} \\ &= \left[\psi_1^n \quad \psi_2^n \quad \cdot \quad \cdot \quad \psi_n^n\right] \hat{\mathbf{u}} \end{aligned} \tag{10}$$

In Eqn. 10, the column vector $\boldsymbol{\Psi}_n(\mathbf{r})$ is defined as

$$\boldsymbol{\Psi}_n(\mathbf{r}) = \left(\boldsymbol{\Phi}_n\right)^{-1} \boldsymbol{\varphi}_n(\mathbf{r}) = \left[\psi_1^n \quad \psi_2^n \quad \cdot \quad \cdot \quad \psi_n^n\right]^T \tag{11}$$

The functions ψ_i^n, i=1,...,n are the shape functions for the LMQ interpolation. It can be easily proved that ψ_i^n satisfies the Kronecker delta condition

$$\psi_i^n(\mathbf{x}_j) = \begin{cases} 1 & \text{if } i = j \\ 0 & \text{otherwise} \end{cases} \quad \text{for } i, j = 1,...,n \tag{12}$$

which is an attractive feature for the treatment of boundary conditions, especially when used in conjunction with point collocation technique. It should also be noted that the existence of $(\boldsymbol{\Phi}_n)^{-1}$ significantly simplifies the computations of the LMQ shape functions. In actually implementation, when checking the existence of $(\boldsymbol{\Phi}_n)^{-1}$, one only needs to ensure the distinctiveness of the nodal points in the cover and it is not necessary to compute the value of Det($\boldsymbol{\Phi}_n$) which is expensive and usually sensitive to the choice of computing algorithm used and the rounding-off error of the computer.

Obviously, Eqns. 5 to 12 are also valid for the case of LIMQ approximation, in which one needs only to replace the function $\phi(\|\mathbf{r}-\mathbf{r}_i\|,c)$ by $\dfrac{1}{\phi(\|\mathbf{r}-\mathbf{r}_i\|,c)}$.

Once the shape functions of the LMQ and the LIMQ approximations are defined, since the matrix $(\mathbf{\Phi}_n)^{-1}$ does not contain any term of x, y, it is a trivial task to compute their derivatives.

$$\left[\frac{\partial\psi_1^n}{\partial x}\quad\frac{\partial\psi_2^n}{\partial x}\quad .\quad .\quad\frac{\partial\psi_n^n}{\partial x}\right]^T=\frac{\partial\mathbf{\Psi}_n(\mathbf{r})}{\partial x}=(\mathbf{\Phi}_n)^{-1}\frac{\partial\boldsymbol{\varphi}_n(\mathbf{r})}{\partial x}$$
$$\frac{\partial\boldsymbol{\varphi}_n(\mathbf{r})}{\partial x}=\left[\frac{\partial\phi(\|\mathbf{r}-\mathbf{r}_1\|)}{\partial x}\quad .\quad\frac{\partial\phi(\|\mathbf{r}-\mathbf{r}_i\|)}{\partial x}\quad .\quad\frac{\partial\phi(\|\mathbf{r}-\mathbf{r}_n\|)}{\partial x}\right]^T \tag{13}$$

In 2D problems, if LMQ approximation is used, then

$$\frac{\partial\phi(\|\mathbf{r}-\mathbf{r}_i\|)}{\partial x}=\frac{\partial\left(\sqrt{(x-x_i)^2+(y-y_i)^2+c^2}\right)}{\partial x}$$
$$=\frac{(x-x_i)}{\sqrt{(x-x_i)^2+(y-y_i)^2+c^2}} \tag{14}$$

The derivatives with respect to y can be computed in a similar way. From Eqn. 14, one can see that the first (and higher order) derivatives of the shape functions can be computed explicitly at any point in $\Omega_{\mathbf{x}}$.

3. Collocation method and cover schemes

3.1 Solution of boundary value problem (BVP) by collocation using LMQ and LIMQ approximations

Consider the following BVP:

$$L_{2m}u=f \quad \text{in } \Omega \tag{15a}$$

having the following boundary conditions:

$$G_iu=b_i \text{ at boundary } \Gamma_i,\ i=0,...,m-1 \tag{15b}$$

In Eqn. 15, L_{2m} denotes a linear differential operator of order *2m*. u is the solution to be calculated and f is the forcing function. G_i denotes a linear differential operator of order i. Γ_i are the boundaries of the domain such that

$$\Gamma = \bigcup_{i=1}^{m-1} \Gamma_i \tag{16}$$

where Γ is the boundary of the whole problem domain. Note that Γ_0 is the essential boundary of the problem along which the essential boundary condition is given by

$$G_0 u = b_0 \tag{17}$$

When the collocation method is employed in conjunction with the LMQ or the LIMQ approximations to solve Eqn. 15, nodal points are placed in the problem domain and the exact solution u in Eqn. 15 is replaced by the approximated solution $\hat{u}$ such that

$$u(\mathbf{x}) \approx \hat{u}(\mathbf{x}) = \boldsymbol{\Psi}\hat{\mathbf{u}} \tag{18a}$$

In Eqn. 18a, the shape function $\boldsymbol{\Psi}$ and the solution vector $\hat{\mathbf{u}}$ are given by

$$\boldsymbol{\Psi} = \left[\psi_1^{n_1} \quad \cdot \quad \psi_i^{n_i} \quad \cdot \quad \psi_N^{n_N}\right]^T, \quad \hat{\mathbf{u}} = \left[\hat{u}(\mathbf{x}_1) \quad \cdot \quad \hat{u}(\mathbf{x}_i) \quad \cdot \quad \hat{u}(\mathbf{x}_N)\right]^T \tag{18b}$$

In Eqn. 18b, N denotes the total number of nodes in the problem domain. $\psi_i^{n_i}$ is the LMQ or the LIMQ shape function for the i^{th} node ($\mathbf{x}_i$) which is constructed by using Eqns. 1 through 11. n_i and $\hat{u}(\mathbf{x}_i)$ are respectively the number of nodes inside the cover of $\mathbf{x}_i$ and the nodal value of the approximation function at $\mathbf{x}_i$. Note that if n_i=N is set for all nodes in the problem domain, the LMQ and the LIMQ approximations become the *global multiquadric* (GMQ) and the *global inverse multiquadric* (GIMQ) approximations respectively. Consequently, the downstream operations involve inverse of an N×N matrix (Eqn. 10) in the process of constructing the shape functions. Not only it demands a costly computation, but also results in a fully populated coefficient matrix, which often becomes ill-conditioned as N increases [18].

On the other hand, replacing u in Eqns. 15 and 16 by $\hat{u}$ leads to the following linear equations system:

$$\left(L_{2m}\boldsymbol{\Psi}\right)\hat{\mathbf{u}} = \hat{\mathbf{f}} \tag{19a}$$

having the boundary conditions: $(G_i\boldsymbol{\Psi})\hat{\mathbf{u}} = \hat{\mathbf{b}}_i$ for Γ_i, i=0,...,m-1 (19b)

such that

$$\hat{\mathbf{f}} = \left[f(\mathbf{x}_1) \quad f(\mathbf{x}_2) \quad \cdot \quad \cdot \quad f(\mathbf{x}_N)\right]^T \quad \text{and} \quad \hat{\mathbf{b}}_i = \left[b_i(\mathbf{x}_1) \quad b_i(\mathbf{x}_2) \quad \cdot \quad \cdot \quad b_i(\mathbf{x}_{NB_i})\right] \tag{19c}$$

In Eqn. 19c, NB_i denotes the number of nodes along the boundary Γ_i.

Since the LMQ and the LIMQ shape functions $\psi_i^{n_i}$ are local shape functions, if the nodal numbers are sorted in ascending order along the x direction, the left-hand side of Eqn. 19a becomes a banded matrix. Furthermore, since all $\psi_i^{n_i}$ satisfy the Kronecker delta condition, the essential boundary condition along the Γ_0 can be imposed right away in the same manner as in the standard finite element procedures by modifying the corresponding terms in Eqn. 19a. In this regard, it is superior to many other meshless methods, which often needs special treatments to satisfy the essential boundary conditions [20-23].

3.2 Cover schemes

Upon solving the set of linear equations and obtaining the coefficients of the nodal vector $\hat{\mathbf{u}}$, the approximation solution $\hat{u}$ and their derivatives can then be derived from Eqn. 18a, i.e.

$$\hat{u}(\mathbf{x}) = \boldsymbol{\Psi}\hat{\mathbf{u}}, \quad \frac{\partial \hat{u}(\mathbf{x})}{\partial \mathbf{x}} = \frac{\partial \boldsymbol{\Psi}}{\partial \mathbf{x}}\hat{\mathbf{u}} \tag{20}$$

Note that to ensure Eqn. 20 applicable to any point inside the problem domain Ω, the necessary condition is that the assembly of all nodal covers completely embraces the problem domain. That is

$$\Omega = \bigcup_{i=1}^{N} \Omega_{\mathbf{x}_i} \tag{21}$$

Eqn. 21 implies that for any point $\mathbf{x}$ in the problem domain, it must fall inside at least one nodal cover. Furthermore, when evaluating $\hat{u}(\mathbf{x})$ and $\frac{\partial \hat{u}(\mathbf{x})}{\partial \mathbf{x}}$ at an arbitrary $\mathbf{x}$, it is only necessary to get involved those nodes whose cover embraces $\mathbf{x}$. For example in Fig. 2, when evaluating $\hat{u}(\mathbf{x})$ at $\mathbf{x}$, one only needs to consider the nodes $\mathbf{x}_i$ (i=1,...,5) whose cover embraces $\mathbf{x}$, while $\mathbf{x}_6$ is ignored. Hence, $\hat{u}(\mathbf{x})$ is given by

$$\hat{u}(\mathbf{x}) = \sum_{i=1}^{5} \psi_i^{n_i} \hat{u}(\mathbf{x}_i) \tag{22}$$

Against this background, when applying the LMQ or LIMQ to solve BVP, one should be cautious in designing the sizes of all nodal covers. It is an important factor that affects the performance of the method.

Consider a scenario that the problem domain is covered by a constellation of nodes at uniform spacing *h*. Eqn. 21 can be easily satisfied by adopting a uniform cover scheme in which the sizes of all nodal covers are the same. Figs. 3 and 4 show examples of uniform cover schemes used in the current study for 1D and 2D problems respectively. For easy visualisation, Fig. 5 plots the shape functions of the 1D LMQ approximation using the 5-point scheme with h=0.1 and c=0.2.

Consider another scenario that the problem domain is covered by a constellation of non-uniformly spaced nodes. Adopting a single cover-size for all may lead to various extreme cases. For example, there may be too many nodes fallen within a nodal cover in the densely populated zone, or too few fallen within a nodal cover in the sparsely populated zone. To avoid the occurrence of these extreme scenarios, a strategy of assigning variable cover sizes to different nodes is adopted in the current study whenever non-uniform distribution of nodes is encountered. For those cases, the cover size D_i of node $\mathbf{x}_i$ is determined through three steps:

i) Identify the four nearest nodes $\mathbf{x}_j$ (j=1,2,3,4) to $\mathbf{x}_i$ and compute the distances between $\mathbf{x}_i$ and $\mathbf{x}_j$, $\left\|\mathbf{r}_i - \mathbf{r}_j\right\|$ (Fig. 6).

ii) Amongst the four, identify the furthest whose spacing to $\mathbf{x}_i$ is $d_i=\max(\left\|\mathbf{r}_i - \mathbf{r}_j\right\|, j=1,2,3,4)$.

iii) Determine the cover size D_i of $\mathbf{x}_i$ such that

$$D_i=\rho d_i \tag{23}$$

In Eqn. 23, ρ is a constant >1. It ensures that Eqn. 21 is satisfied. Note that a too big value of ρ often leads to a cover having too many nodes fallen inside, and hence jeopardises the accuracy of solution. In addition, a cover embracing too many nodes will definitely increases the bandwidth of the resulting matrix regardless of the nodal numbering sequence, and hence pushes up the computational cost. Therefore in the subsequent numerical studies, a moderate value of 2.0 for ρ is adopted so that the maximum number of nodes in a cover is limited to 20.

4. Numerical examples

Three numerical examples are given to demonstrate the efficiency and accuracy of the present LMQ and LIMQ approximations used in conjunction with collocation techniques. Results are compared with their global counterparts (GMQ and GIMQ). In the numerical studies, various values of the parameter c are used to investigate its effect on the accuracy of the solution.

Furthermore, *h*- refinements are also carried out to study the rate of convergence. In all examples, the errors of the numerical solution are measured by the following relative error indicators:

i) Relative error η for solution u. It is defined as

$$\eta = \sqrt{\frac{\sum_{i=1}^{N}\left(u(\mathbf{x}_i) - \hat{u}(\mathbf{x}_i)\right)^2}{\sum_{i=1}^{N} u(\mathbf{x}_i)^2}} \tag{24}$$

ii) Relative errors η_x and η_y for the derivatives $\frac{\partial u}{\partial x}$ and $\frac{\partial u}{\partial y}$. They are defined as

$$\eta_x = \sqrt{\frac{\sum_{i=1}^{N}\left(\frac{\partial u(\mathbf{x}_i)}{\partial x} - \frac{\partial \hat{u}(\mathbf{x}_i)}{\partial x}\right)^2}{\sum_{i=1}^{N}\left(\frac{\partial u(\mathbf{x}_i)}{\partial x}\right)^2}} \quad \text{and} \quad \eta_y = \sqrt{\frac{\sum_{i=1}^{N}\left(\frac{\partial u(\mathbf{x}_i)}{\partial y} - \frac{\partial \hat{u}(\mathbf{x}_i)}{\partial y}\right)^2}{\sum_{i=1}^{N}\left(\frac{\partial u(\mathbf{x}_i)}{\partial y}\right)^2}} \tag{25}$$

The convergence rate of the relative errors is denoted by $R(\xi)$ (for $\xi=\eta$, η_x or η_y), which is defined as

$$R(\xi) = \frac{\log(\frac{\xi_i}{\xi_{i+1}})}{\log(\frac{h_i}{h_{i+1}})} \tag{26a}$$

In Eqn. 26, ξ and h are respectively the relative error and the nodal spacing. The subscripts 'i' and 'i+1' denote two consecutive uniform *h*-refinements. It can be shown that when the LMQ and LIMQ schemes are used *with sufficiently large* covers sizes, the converge rates are given by [16,17]

$$R(\eta) = O(h^{ND+1}) \quad \text{and} \quad R(\eta_x) = O(h^{ND}), \quad R(\eta_y) = O(h^{ND}) \tag{26b}$$

where ND is the spatial dimension.

4.1 Example 1: 1D Poisson equation

A 1-D Poisson equation is solved using LMQ approximation. The accuracy is illustrated through different cover schemes and progressive uniform *h*-refinement as well. The governing differential equation and boundary conditions are

$$\frac{\partial^2 u}{\partial x^2} = \frac{105}{2}x^2 - \frac{15}{2}, \quad \Omega = [-1,1] \quad \text{and} \quad u(x = \pm 1) = 1 \tag{27}$$

The exact solution for this problem is given by

$$u = \frac{35}{8}x^4 - \frac{15}{4}x^2 + \frac{3}{8} \tag{28}$$

This problem is analysed using three different sets of nodes totalling 21, 41 and 81 nodes at even spacing of h=0.1, 0.05 and 0.025 respectively. Different ways of constructing the LMQ approximations are adopted. They are: i) 3-point cover scheme with h=0.1, various c (0.1, 0.4 or 0.8); ii) 5-point cover scheme with h=0.05, various c (0.1, 0.4 or 0.8); and iii) 7-point cover scheme with h=0.025, various c (0.1, 0.4 or 0.8). Totally 9 analyses (3 cover schemes × 3 c values) are carried out. The results for 5-point cover scheme (with nodal spacing h=0.05) and various values of c are shown in Fig. 7. It can be seen from Fig. 7 that when c=0.1, the computed solution is almost equal to the exact solution. In fact, a more detailed analysis shows that when c=0.1, the computed solutions are almost identical with the exact solution for all the values of h (0.1, 0.05 and 0.025) and all cover schemes tested. In addition, the results obtained by using c=0.4 and 0.8 are very similar in all cases. Based on these observations, the study of the influence cover scheme on the accuracy and the convergence rate of solution is conducted only for the case of c=0.4. Tables 1 and 2 list the relative errors η and η_x under various cover schemes but having same c value (0.4). It can be seen that, in terms of both accuracy and convergence rate, the 7-point cover scheme appears to be the best performer. Furthermore, Eqn. 26b is confirmed and it is interested to see that for the 5-point and 7-points cases, the convergence rates even exceeds the rate given by Eqn. 26b.

4.2 Example 2: 2D Possion Equation with Dirichlet boundary condition

Consider a 2D Possion equation of the form

$$\nabla^2 u = \sin(\pi x)\sin(\pi y) \tag{29}$$

over a unit square $(x,y) \in [0,1] \times [0,1]$ subjects to the Dirichlet condition u=0 along the whole domain boundary. The exact solution is given by

$$u(x, y) = \frac{-\sin(\pi x)\sin(\pi y)}{2\pi^2} \tag{30}$$

This problem is analysed using a constellation of 121 nodal points, which are either uniformly or non-uniformly distributed over the square domain. In the analysis with uniform nodal distribution (Fig. 8), the nodal spacing is h=0.1 and 25-point cover scheme (Fig. 4c) is used. In the analysis using non-uniform nodal distribution (Fig. 9), the variable cover scheme described in Section 3 with ρ=2.0 is used. In each analysis, solutions are obtained separately through four different approximation strategies in conjunction with collocation techniques. The four strategies are: LMQ, LIMQ, GMQ, and GIMQ. In addition, values of the parameter 'c' are varied ranging from 0.1 to 1.5 in each of the four strategies. Their effects on the accuracy of solution are observed and measured in terms of relative errors. Tables 3 and 4 list the relative errors occurred in the uniform and non-uniform nodal model respectively. For easy visualization, it is also plotted in Figs. 10 and 11.

From Tables 3 and 4 and Figs. 10 and 11, it is interesting to note that,

i) Amongst the 4 approximation strategies, be it applied over the uniform or non-uniform nodal model, when the parameter *c* is set to a particular value (c=0.8), the GMQ strategy yields the most accurate results, and the GIMQ comes second.

ii) However, the performance of two global approximation strategies (GMQ and GIMQ) deteriorates quickly when the value of c deviates from that particular magic value. On the contrary, the two local approximation strategies (LMQ and LIMQ) are found much less sensitive to the value of c than their global counterparts. Be it applied over the uniform or non-uniform nodal model, both LMQ and LIMQ are able to yield reasonably accurate results with the relatively error indicator $\eta \leq 2\%$ whenever $c>0.3$.

iii) Although the LMQ and LIMQ strategies do not always yield result more accurate than their global counterparts at the chosen magic value of *c*, they possess other qualities which render it more attractive. Particularly, it saves lots of computational cost in the process of constructing the shape functions. In the GMQ and the GIMQ formulations, the process involves matrix inversion operations of the order equal to the total number of nodes in the whole constellation. It is much more expensive than those in the local formulations, which require only inversion operations of much lower-order matrices.

To study the convergence characteristics of the LMQ and the LIMQ strategies, the 5-, 9- and 25-nodal cover schemes (Fig. 4) are applied separately over three uniformly distributed nodal constellations. Total number of nodes equals to NR×NR (Fig. 8). When NR=6, the nodal spacing

h=0.2; when NR=11, h=0.1; and when NR=21, h=0.05. A value 0.4 is chosen for the parameter *c*. The convergence rates η and η_x measured for LMQ for LIMQ against different cover schemes are shown in Tables 5 and 6 respectively. From Tables 5 and 6, it can be seen that in both LMQ and LIMQ, the largest size 25-point cover scheme yields the most accurate results and the convergence rates predicted by Eqn. 26b. In general, the performance of the LMQ strategy is slightly better than the LIMQ. Regarding the convergence rates, both LMQ and LIMQ tend to have higher convergence rates with increasingly refined (or more densely populated) nodal constellation.

4.3 Example 3: 2D Possion Equation with both Dirichlet and Neumann boundary conditions

Consider a 2D Possion equation of the form

$$\nabla^2 u = 13e^{(2x+3y)} \tag{31}$$

defined over a unit square domain $(x,y)\in[0,1]\times[0,1]$ with both Dirichlet and Neumann boundary conditions given by

$$u = e^{(2x+3y)} \quad \text{along the edges} : y = 0 \text{ and } y = 1 \tag{32a}$$

$$\frac{\partial u}{\partial x} = 2e^{(2x+3y)} \quad \text{along the edges} : x = 0 \text{ and } x = 1 \tag{32b}$$

The exact solution of the problem is given by

$$u(x, y) = e^{(2x+2y)} \tag{33}$$

Similar to Example 2, this problem is analysed using a constellation of 121 nodal points, which are either uniformly or non-uniformly distributed over the square domain. In the analysis with uniform nodal distribution (Fig. 8), the nodal spacing is h=0.1 and 25-point cover scheme (Fig. 4c) is used. In the analysis using non-uniform nodal distribution (Fig. 9), the variable cover scheme described in Section 3 with ρ=2.0 is used. In each analysis, the four strategies (LMQ, LIMQ, GMQ, and GIMQ) are employed to obtain solutions against various values of *c* ranging from 0.1 to 1.5. Their effects on the accuracy of solution are observed and measured in terms of relative errors. Tables 7 and 8 list the relative errors occurred in the uniform and non-uniform nodal model respectively. For easy visualization, it is also plotted in Figs. 12 and 13. Similar trends in the results as previous examples are observed. In some cases, the global approximation strategies yield more accurate solutions than their local counterparts. However in general, the

local approximation strategies are more stable, insensitive to the value of c and computationally less costly. Furthermore amongst the two local approximation strategies, when measured in terms of accuracy and stability, the LMQ is superior to the LIMQ.

Regarding the convergence characteristics of the LMQ strategy, the 5-, 9- and 25-nodal cover schemes (Fig. 4) are applied separately over three uniformly distributed nodal constellations, in which the total numbers of nodes are 6x6, 11x11 and 21x21 respectively. A value 0.2 is chosen for the parameter c. The convergence rates η and η_x against different cover schemes are shown in Tables 9a and 9b respectively. From Table 9, similar to Example 2, it can be seen that the 25-point scheme again yields the most accurate solution and highest convergence rates.

5. Conclusions

In this paper, new approximation strategies for solving BVPs using the local multiquadric (LMQ) and the local inverse multiquadric (LIMQ) are presented. Different from many available global approximation strategies such as GMQ, GIMQ, or other radial basis functions, the present approximation strategy is a pure local procedure. In constructing the shape function for a given node $\mathbf{x}_i$, it only involves nodes fallen within its influence (cover) zone. The existence of such shape functions is guaranteed, provided that all nodes are distinct points and the free parameter c is assigned a positive value. It is the distinct feature superior to many other meshless approximation strategies, including the popular moving-least-square method, which fails in the process of constructing the shape function in some cases having arbitrary nodal distributions. Another major advantage of the present strategy is the easiness in imposing essential boundary conditions, because the shape functions satisfy the Kronecker delta condition strictly. It requires no special treatments at all.

The effectiveness of the present LMQ and LIMQ approximation strategies are demonstrated through solving 1D and 2D BVPs in conjunction with collocation technique. The numerical studies show that they often outperform their global counterparts (GMQ and GIMQ), particularly with regard to viability and stability. They yield accurate solutions and the procedure remains stable over a wide range of values of the free parameter c.

References

1. T. Belytschko, Y. Y. Lu and L. Gu, Element-free Galerkin method, Int. J. Numer. Methods Engrg., **37,** 229-256 (1984)

2. T. Belytschko, Y. Krongauz, D. Organ, M. Fleming and P. Krysl: Meshless methods: An overview and recent developments, Comput. Methods Appl. Mech. Engrg., **139,** 3-47, (1996)

3. W. K. Liu, Y. Chen, C. T. Chang and T. Belytschko: Advances in multiple scale kernel particle methods, Comput. Mech., **18,** 73-111 (1996)

4. W. K. Liu, S. Jun, S. F. Li, J. Adee and T. Belytschko, Reproducing kernel particle methods for structural dynamics, Int. J. Numer. Methods Engrg., **38,** 1655-1679 (1995)

5. J. T. Oden, C. A. Duarte and O. C. Zienkiewicz: A new Cloud-Based hp finite element method, Int. J. Numer. Methods Engrg., **50,** 160-170, (1998)

6. I. Babuska and J. M. Melenk: The partition of unity method, Int. J. Numer. Methods Engrg., **40**, 727-758, (1997)

7. S. N. Atluri, T. Zhu, A new meshless local Petrov-Galerkin (MLPG) approach in computational mechanics, Comput. Mech. **22**, 117-127, (1998)

8. G. R. Liu, Y. T. Gu, A point interpolation method for two-dimensional solids, Int. J. Numer. Methods Engrg, **50**, 937-951, (2001)

9. E. Onate, S. Idelsohn, O. C. Zienkiewicz, R. L. Taylor A finite point method in computational mechanics. Applications to convective Transport and fluid flow, Int. J. Numer. Methods Engrg, **39**, 3839-3866, (2001)

10. X. Liu, Application of Finite Point Method in Reservoir Simulation and Numerical Simulation of Option Pricing Models, Research Report of Post-Doctoral Fellow, Tsinghua University, **6**, (2000)

11. N. R. Aluru and G. Li, Finite cloud method: a true meshless technique based on a fixed reproducing kernel approximation, Int. J. Numer. Meth. Engng., **50**, 2373-2410, (2001)

12. R. L. Hardy, Multiquadric equations of topography and other irregular surfaces. Journal of Geophysics Res.176, 1905 –1915, (1971)

13. R. Franke, Scattered data interpolation: test of some methods. Mathematics of Computation, **38**, 181-200, (1982)

14. E.J. Kansa, Multiquadrics: a scattered data approximation scheme with applications to computational fluid-dynamics. Comput. Math. and Appl. **19**, 147-161, (1990)

15. Y.C. Hon, M. W. Lu, et al., Multiquadric method for the numerical solution of a biphasic mixture model, Appl. Math. Comp. **88**, 153-175, (1997)

16. M. A. Golberg, C. S. Chen and S. R. Karur, Improved multiquadrics approximation for partial differential equations, Engineering Analysis with Boundary Elements, **18**, 9-17, (1996)

17. M. A. Golberg, C. S. Chen, A bibliography on radial basis function approximations. Boundary Elements Communications, **7**, 155-163, (1996)

18. E. J. Kansa and Y. C. Hon, Circumventing the Ill-Conditioning Problem with Multiquadric Radial Basis Functions: Applications to Elliptic Partial Differential Equations, Computers and Math. Appl., **39**, 123-137, (2000)

19. N. Sukumar, B. Maran and T. Belytschko, The natural element method in solid mechanics, Int. J. Numer. Methods Engrg., **43,** 839-887 (1998)

20. Y. Y. Lu, T. Belytschko, L. Gu, "A New Implementation of the Element Free Galerkin Method", Comput. Methods Appl. Mech. Engrg., **113**, 397-414 (1994)

21. Y. Krongauz , T. Belytschko, "Enforcement of Essential Boundary Conditions in Meshless Approximations Using Finite Elements", Comput. Methods Appl. Mech. Engrg., **131**,133-145 (1996)

22. T. Belytschko, D. Organ, Y. Krongauz, "A Coupled Finite Element-Element Free Galerkin Method", Computational Mechanics, **17**, 186-195 (1995)

23. C. K. Wu and M. E. Plesha, "Essential boundary condition enforcement in meshless methods: boundary flux collocation method", Int. J. Numer. Meth. Engng., **53**, 499-514, (2002)

Appendix: Proof for the existence of $(\boldsymbol{\Phi}_n)^{-1}$

In order to prove the existence of $(\boldsymbol{\Phi}_n)^{-1}$, one needs to first establish the following lemmas.

Lemma 1: For the vector function $\boldsymbol{\varphi}_n(\mathbf{r})$ defined in Eqn. 7 corresponding to an arbitrary point $\mathbf{x}$, if $\boldsymbol{\varphi}_n(\mathbf{r}) = \pm\boldsymbol{\varphi}_n(\mathbf{r}_i)$ for any i=1,...,n, then $\mathbf{x}=\mathbf{x}_i$.

Proof

By the definition of $\boldsymbol{\varphi}_n(\mathbf{r})$, if $\boldsymbol{\varphi}_n(\mathbf{r}) = \boldsymbol{\varphi}_n(\mathbf{r}_i)$, then one can write

$$\begin{bmatrix} \phi(\|\mathbf{r}-\mathbf{r}_1\|,c) \\ \phi(\|\mathbf{r}-\mathbf{r}_2\|,c) \\ \cdot \\ \phi(\|\mathbf{r}-\mathbf{r}_i\|,c) \\ \cdot \\ \phi(\|\mathbf{r}-\mathbf{r}_n\|,c) \end{bmatrix} = \pm \begin{bmatrix} \phi(\|\mathbf{r}_i-\mathbf{r}_1\|,c) \\ \phi(\|\mathbf{r}_i-\mathbf{r}_2\|,c) \\ \cdot \\ \phi(\|\mathbf{r}_i-\mathbf{r}_i\|,c) \\ \cdot \\ \phi(\|\mathbf{r}_i-\mathbf{r}_n\|,c) \end{bmatrix} \tag{A1}$$

Consider the i^{th} component of Eqn. A1 and the definition of $\phi(\|\mathbf{r}-\mathbf{r}_i\|,c)$ for the LMQ approximation (Eqn. 2), one can write

$$\begin{aligned} \phi(\|\mathbf{r}-\mathbf{r}_i\|,c) &= \pm\phi(\|\mathbf{r}_i-\mathbf{r}_i\|,c) \\ \Rightarrow \sqrt{\|\mathbf{r}-\mathbf{r}_i\|^2+c^2} &= \pm\sqrt{\|\mathbf{r}_i-\mathbf{r}_i\|^2+c^2} \\ \Rightarrow \|\mathbf{r}-\mathbf{r}_i\|^2 &= 0 \\ \Rightarrow \mathbf{x} &= \mathbf{x}_i \end{aligned} \tag{A2}$$

Lemma 2: $\boldsymbol{\varphi}_n(\mathbf{r}_i)$, i=1,...,n are n independent vectors if $(\boldsymbol{\Phi}_n)^{-1}$ exist.

Proof

Proof for the linearly independence of $\boldsymbol{\varphi}_n(\mathbf{r}_i)$, i=1,...,n can be simply done by observing the fact that

$$\boldsymbol{\Phi}_n = \begin{bmatrix} \boldsymbol{\varphi}_n(\mathbf{r}_1) & \boldsymbol{\varphi}_n(\mathbf{r}_2) & \cdot & \cdot & \boldsymbol{\varphi}_n(\mathbf{r}_n) \end{bmatrix} = \begin{bmatrix} \boldsymbol{\varphi}_n(\mathbf{r}_1)^T \\ \boldsymbol{\varphi}_n(\mathbf{r}_2)^T \\ \cdot \\ \cdot \\ \boldsymbol{\varphi}_n(\mathbf{r}_n)^T \end{bmatrix} \tag{9}$$

Hence, if $(\boldsymbol{\Phi}_n)^{-1}$ exists, $\boldsymbol{\varphi}_n(\mathbf{r}_i)$, i=1,...,n must be linear independent.

Lemma 3: For an arbitrary point $\mathbf{x}$ and an integer n>0, if $(\mathbf{\Phi}_n)^{-1}$ exists and $\boldsymbol{\varphi}_n(\mathbf{r})^T(\mathbf{\Phi}_n)^{-1}\boldsymbol{\varphi}_n(\mathbf{r}) = c$, then $\mathbf{x}=\mathbf{x}_i$ for an integer i such that $1 \le i \le n$.

Proof

Since $\mathbf{\Phi}_n$ is not singular, consider the vector $\mathbf{p}_i = (\mathbf{\Phi}_n)^{-1}\boldsymbol{\varphi}_n(\mathbf{r}_i), 1 \le i \le n$. From Eqn. 11, one can write

$$\begin{aligned}\mathbf{p}_i &= (\mathbf{\Phi}_n)^{-1}\boldsymbol{\varphi}_n(\mathbf{r}_i), 1 \le i \le n \\ &= \left[\psi_1^n(\mathbf{x}_i) \quad \cdot \quad \psi_i^n(\mathbf{x}_i) \quad \cdot \quad \psi_n^n(\mathbf{x}_i)\right]^T \\ &= \left[0 \quad \cdot \quad \psi_i^n(\mathbf{x}_i) \quad \cdot \quad 0\right]^T \\ &= \left[0 \quad \cdot \quad \underset{\text{ith component}}{1} \quad \cdot \quad 0\right]^T\end{aligned} \tag{A3a}$$

and obviously,

$$(\mathbf{p}_i)^T\mathbf{\Phi}_n\mathbf{p}_i = c \quad \text{and} \quad \mathbf{\Phi}_n\mathbf{p}_i = \boldsymbol{\varphi}_n(\mathbf{r}_i) \tag{A3b}$$

Furthermore, for any $\boldsymbol{\varphi}_n(\mathbf{r})$, there exists a vector $\mathbf{q}$ such that

$$\mathbf{\Phi}_n\mathbf{q} = \boldsymbol{\varphi}_n(\mathbf{r}) \quad \text{or} \quad \mathbf{q} = (\mathbf{\Phi}_n)^{-1}\boldsymbol{\varphi}_n(\mathbf{r}) \tag{A4}$$

Since $\mathbf{x}$ is arbitrary, so are $\boldsymbol{\varphi}_n(\mathbf{r})$ and $\mathbf{q}$. Therefore, one can always write

$$\mathbf{q} = \mathbf{p}_i + \mathbf{w} \quad \text{for } 1 \le i \le n \tag{A5}$$

such that $\mathbf{w}$ is another arbitrary vector.

Now, consider the condition

$$\begin{aligned}c &= \boldsymbol{\varphi}_n(\mathbf{r})^T(\mathbf{\Phi}_n)^{-1}\boldsymbol{\varphi}_n(\mathbf{r}) \\ &= \boldsymbol{\varphi}_n(\mathbf{r})^T(\mathbf{\Phi}_n)^{-1}\mathbf{\Phi}_n(\mathbf{\Phi}_n)^{-1}\boldsymbol{\varphi}_n(\mathbf{r}) \\ &= \mathbf{q}^T\mathbf{\Phi}_n\mathbf{q} \quad \text{(using Eqn. A4)} \\ &= (\mathbf{p}_i + \mathbf{w})^T\mathbf{\Phi}_n(\mathbf{p}_i + \mathbf{w}) \quad \text{(using Eqn. A5)} \\ &= (\mathbf{p}_i)^T\mathbf{\Phi}_n\mathbf{p}_i + (\mathbf{p}_i)^T\mathbf{\Phi}_n\mathbf{w} + \mathbf{w}^T\mathbf{\Phi}_n\mathbf{p}_i + \mathbf{w}^T\mathbf{\Phi}_n\mathbf{w} \\ &= c + 2\mathbf{w}^T\mathbf{\Phi}_n\mathbf{p}_i + \mathbf{w}^T\mathbf{\Phi}_n\mathbf{w} \\ &= c + 2\mathbf{w}^T\boldsymbol{\varphi}_n(\mathbf{r}_i) + \mathbf{w}^T\mathbf{\Phi}_n\mathbf{w} \quad \text{(using Eqn. A3b)}\end{aligned} \tag{A6}$$

The last line of Eqn. A6 implies that

$$0 = 2\mathbf{w}^{\mathsf{T}}\boldsymbol{\varphi}_n(\mathbf{r}_i) + \mathbf{w}^{\mathsf{T}}\boldsymbol{\Phi}_n\mathbf{w} \quad \text{or} \quad \mathbf{w}^{\mathsf{T}}\left(2\boldsymbol{\varphi}_n(\mathbf{r}_i) + \boldsymbol{\Phi}_n\mathbf{w}\right) = 0 \tag{A7}$$

From Eqn. A7, two possible cases should be considered:

Case I: $\left(2\boldsymbol{\varphi}_n(\mathbf{r}_i) + \boldsymbol{\Phi}_n\mathbf{w}\right) \neq \mathbf{0}$ for all i=1,...,n.

In such a case, since **w** is arbitrary, one may set

$$\left(2\boldsymbol{\varphi}_n(\mathbf{r}_i) + \boldsymbol{\Phi}_n\mathbf{w}\right) = \mathbf{v}_i \tag{A8}$$

By using Eqn. A7 and setting i=1,...,n, for Eqn. A8, it can be concluded that

$$\mathbf{w}^{\mathsf{T}}\mathbf{v}_i = 0 \quad \text{for i=1,...,n} \tag{A9}$$

Note that $\mathbf{v}_i$, i=1,...,n are n independent vectors because from Eqn. A8, for any integers i,j such that $1 \le i,j \le n$

$$\begin{aligned}\mathbf{v}_i - \mathbf{v}_j &= \left(2\boldsymbol{\varphi}_n(\mathbf{r}_i) + \boldsymbol{\Phi}_n\mathbf{w}\right) - \left(2\boldsymbol{\varphi}_n(\mathbf{r}_j) + \boldsymbol{\Phi}_n\mathbf{w}\right) \\ &= 2(\boldsymbol{\varphi}_n(\mathbf{r}_i) - \boldsymbol{\varphi}_n(\mathbf{r}_j))\end{aligned} \tag{A10}$$

and from Lemma 2, $\boldsymbol{\varphi}_n(\mathbf{r}_i)$, i=1,...,n are n independent vectors.

Hence, the vector **w** is orthogonal to n independent vectors and therefore one may conclude that **w**=**0**. From Eqn. A5, this implies that

$$\mathbf{q} = \mathbf{p}_i \quad \text{for } 1 \le i \le n \tag{A11a}$$

Therefore, from Eqns. A4 and A3b,

$$\boldsymbol{\Phi}_n\mathbf{q} = \boldsymbol{\varphi}_n(\mathbf{r}) \Rightarrow \boldsymbol{\Phi}_n\mathbf{p}_i = \boldsymbol{\varphi}_n(\mathbf{r}) \Rightarrow \boldsymbol{\varphi}_n(\mathbf{r}) = \boldsymbol{\varphi}_n(\mathbf{r}_i) \tag{A11b}$$

Thus, $\mathbf{x}=\mathbf{x}_i$ from Lemma 1.

Case II: $\left(2\boldsymbol{\varphi}_n(\mathbf{r}_i) + \boldsymbol{\Phi}_n\mathbf{w}\right) = \mathbf{0}$ for at least one $1 \le i \le n$.

In this case, since $\boldsymbol{\Phi}_n$ is not singular, one can obtain **w** as

$$\begin{aligned}\mathbf{w} &= -2\left(\boldsymbol{\Phi}_n\right)^{-1}\boldsymbol{\varphi}_n(\mathbf{r}_i) \\ &= -2\mathbf{p}_i\end{aligned} \tag{A12}$$

Now from Eqns. A4 and A5,

$$\begin{aligned} \mathbf{q} &= \mathbf{p}_i + \mathbf{w} = -\mathbf{p}_i \\ \varphi_n(\mathbf{r}) &= \mathbf{\Phi}_n \mathbf{q} = -\mathbf{\Phi}_n \mathbf{p}_i = -\varphi_n(\mathbf{r}_i) \end{aligned} \tag{A13}$$

and once again, from Lemma 1, $\mathbf{x}=\mathbf{x}_i$.

Proof for the existence of $(\mathbf{\Phi}_n)^{-1}$

The existence of $(\mathbf{\Phi}_n)^{-1}$ can be proved by induction.

First of all, consider the case that n=1 so that $\mathbf{\Phi}_n$ reduces to a single term c and $(\mathbf{\Phi}_n)^{-1}$=1/c exist since c≠0. Furthermore, the shape function $\mathbf{\Psi}_1(\mathbf{r})$ (Eqn. 11) becomes

$$\mathbf{\Psi}_1(\mathbf{r}) = \left[\psi_1^1\right] = \frac{\phi\left(\left\|\mathbf{r} - \mathbf{r}_1\right\|, c\right)}{c} \tag{A14}$$

which obviously satisfies the Kronecker delta condition.

Now consider the case that n=2, for two distinct points $\mathbf{x}_1$ and $\mathbf{x}_2$. The matrix $\mathbf{\Phi}_2$ is given by

$$\mathbf{\Phi}_2 = \begin{bmatrix} c & \sqrt{\left\|\mathbf{r}_1 - \mathbf{r}_2\right\|^2 + c^2} \\ \sqrt{\left\|\mathbf{r}_1 - \mathbf{r}_2\right\|^2 + c^2} & c \end{bmatrix} \tag{A15}$$

Det($\mathbf{\Phi}_2$) can be computed as

$$\begin{aligned} \mathrm{Det}(\mathbf{\Phi}_2) &= c^2 - \left\|\mathbf{r}_1 - \mathbf{r}_2\right\|^2 - c^2 \\ &= -\left\|\mathbf{r}_1 - \mathbf{r}_2\right\|^2 \\ &\neq 0 \quad \text{since } \mathbf{x}_1 \text{ and } \mathbf{x}_2 \text{ are two distinct points} \end{aligned} \tag{A16}$$

Thus, $(\mathbf{\Phi}_2)^{-1}$ exists and is given by

$$\left(\mathbf{\Phi}_2\right)^{-1} = \frac{1}{-\left\|\mathbf{r}_1 - \mathbf{r}_2\right\|^2} \begin{bmatrix} c & -\sqrt{\left\|\mathbf{r}_1 - \mathbf{r}_2\right\|^2 + c^2} \\ -\sqrt{\left\|\mathbf{r}_1 - \mathbf{r}_2\right\|^2 + c^2} & c \end{bmatrix} \tag{A17}$$

The shape functions $\Psi_2(\mathbf{r})$ are therefore given by

$$\Psi_2(\mathbf{r}) = \begin{bmatrix} \psi_1^2 & \psi_2^2 \end{bmatrix}$$

$$\psi_1^2 = \frac{\sqrt{\|\mathbf{r}-\mathbf{r}_2\|^2 + c^2}\sqrt{\|\mathbf{r}_1-\mathbf{r}_2\|^2 + c^2} - c\sqrt{\|\mathbf{r}-\mathbf{r}_1\|^2 + c^2}}{\|\mathbf{r}_1-\mathbf{r}_2\|^2} \tag{A18a}$$

$$\psi_2^2 = \frac{\sqrt{\|\mathbf{r}-\mathbf{r}_1\|^2 + c^2}\sqrt{\|\mathbf{r}_1-\mathbf{r}_2\|^2 + c^2} - c\sqrt{\|\mathbf{r}-\mathbf{r}_2\|^2 + c^2}}{\|\mathbf{r}_1-\mathbf{r}_2\|^2}$$

Obviously, both ψ_1^2 and ψ_2^2 satisfy the Kronecker delta condition.

To complete the proof, for any arbitrary integer n, assume that $(\mathbf{\Phi}_k)^{-1}$ exists and $\psi_i^k(\mathbf{x}_j) = \delta_{ij}$ for i,j =1,...,k. Now consider the matrix $\mathbf{\Phi}_{k+1}$ corresponding to k+1 distinct points $\{\mathbf{x}_1, \mathbf{x}_2,...,\mathbf{x}_k, \mathbf{x}_{k+1}\}$ and the free parameter c. By definition, $\mathbf{\Phi}_{k+1}$ is given by

$$\mathbf{\Phi}_{k+1} = \begin{bmatrix} c & \phi(\|\mathbf{r}_1-\mathbf{r}_2\|,c) & \cdot & \phi(\|\mathbf{r}_1-\mathbf{r}_k\|,c) & \phi(\|\mathbf{r}_1-\mathbf{r}_{k+1}\|,c) \\ \phi(\|\mathbf{r}_1-\mathbf{r}_2\|,c) & c & & \phi(\|\mathbf{r}_2-\mathbf{r}_k\|,c) & \phi(\|\mathbf{r}_2-\mathbf{r}_{k+1}\|,c) \\ \cdot & & \cdot & & \cdot \\ \phi(\|\mathbf{r}_1-\mathbf{r}_k\|,c) & \phi(\|\mathbf{r}_2-\mathbf{r}_k\|,c) & & c & \phi(\|\mathbf{r}_k-\mathbf{r}_{k+1}\|,c) \\ \phi(\|\mathbf{r}_1-\mathbf{r}_{k+1}\|,c) & \phi(\|\mathbf{r}_2-\mathbf{r}_{k+1}\|,c) & \cdot & \phi(\|\mathbf{r}_k-\mathbf{r}_{k+1}\|,c) & c \end{bmatrix} \tag{A19}$$

$$= \begin{bmatrix} \mathbf{\Phi}_k & \varphi_k(\mathbf{r}_{k+1}) \\ \varphi_k(\mathbf{r}_{k+1})^T & c \end{bmatrix}$$

Consider the matrix **B** such that

$$\mathbf{\Phi}_{k+1}\mathbf{B} = \mathbf{B}\mathbf{\Phi}_{k+1} = \mathbf{I}_{k+1} \text{ and } \mathbf{B} = \begin{bmatrix} \underset{(k\times k)}{\mathbf{B}_{11}} & \underset{(k\times 1)}{\mathbf{B}_{12}} \\ \underset{(1\times k)}{(\mathbf{B}_{12})^T} & \underset{(1\times 1)}{B_{22}} \end{bmatrix} \tag{A20}$$

By using Eqns. A19 and A20, it can be easily shown that the submatrices $\mathbf{B}_{11}$, $\mathbf{B}_{12}$ and the term B_{22} are given by

$$\begin{aligned} \mathbf{B}_{11} &= (\mathbf{\Phi}_k)^{-1} + \left((\mathbf{\Phi}_k)^{-1}\varphi_k(\mathbf{r}_{k+1})\right)\alpha^{-1}\left(\varphi_k(\mathbf{r}_{k+1})^T(\mathbf{\Phi}_k)^{-1}\right) \\ \mathbf{B}_{12} &= -\alpha^{-1}\left((\mathbf{\Phi}_k)^{-1}\varphi_k(\mathbf{r}_{k+1})\right) \\ B_{22} &= \alpha^{-1} \\ \alpha &= c - \varphi_k(\mathbf{r}_{k+1})^T(\mathbf{\Phi}_k)^{-1}\varphi_k(\mathbf{r}_{k+1}) \end{aligned} \tag{A21}$$

Since $\left(\boldsymbol{\Phi}_k\right)^{-1}$ exist, if $\alpha \neq 0$, then one can always compute $\mathbf{B}$ such that $\mathbf{B} = \left(\boldsymbol{\Phi}_{k+1}\right)^{-1}$ using Eqn. A21.

Now assume that $\alpha=0$. From the last line of Eqn. A21, it implies

$$\begin{aligned} c &= \boldsymbol{\varphi}_k(\mathbf{r}_{k+1})^T \left(\boldsymbol{\Phi}_k\right)^{-1} \boldsymbol{\varphi}_k(\mathbf{r}_{k+1}) \\ &\Rightarrow \mathbf{x}_{k+1} = \mathbf{x}_i \quad \text{for } 1 \le i \le k, \text{ from } \textbf{Lemma } 3 \end{aligned} \tag{A22}$$

Hence, $\alpha=0$ only when $\mathbf{x}_{k+1}=\mathbf{x}_i$ for $1 \le i \le k$ which contradicts the assumption that the set $\{\mathbf{x}_1, \mathbf{x}_2,...,\mathbf{x}_k, \mathbf{x}_{k+1}\}$ are k+1 distinct points. Thus, one can conclude that $\alpha \neq 0$ and $\mathbf{B} = \left(\boldsymbol{\Phi}_{k+1}\right)^{-1}$ always exists and this completes the proof for the existence of $\left(\boldsymbol{\Phi}_n\right)^{-1}$ in general.

Obviously, the above proof is also valid if the LMQ approximation is replaced by the LIMQ approximation.

Preprint version of the paper in Computational Mechanics, Vol. 30, Issue 5-6, pp 396-409 (2003)

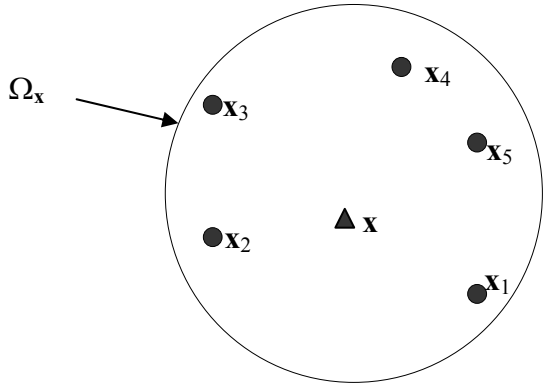

Fig. 1. Influence domain Ω_x of a node **x** embracing 5 neighbouring nodes (n=5).

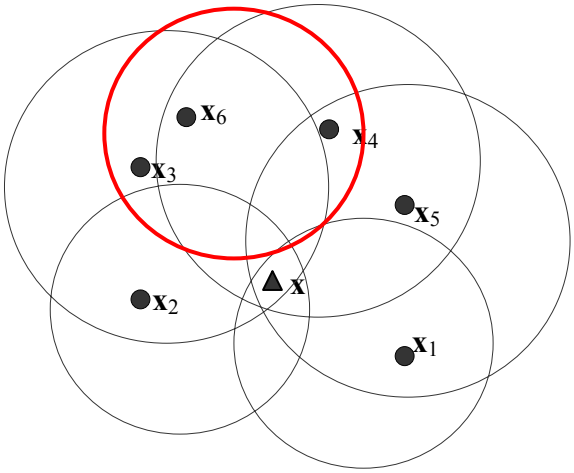

Fig. 2 A location falls within the influence zones of 5 nodes (excluding node $\mathbf{x_6}$).

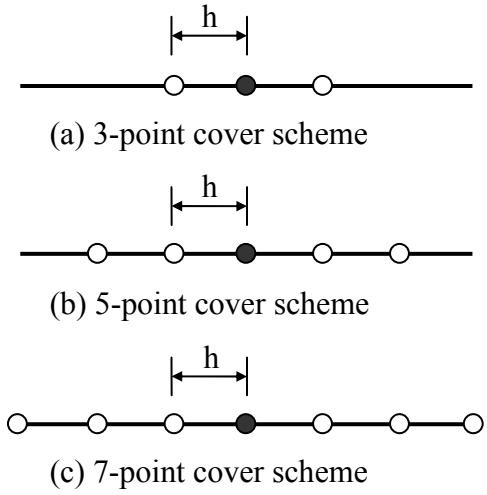

(a) 3-point cover scheme

(b) 5-point cover scheme

(c) 7-point cover scheme

Fig. 3 Cover schemes for 1D problem.

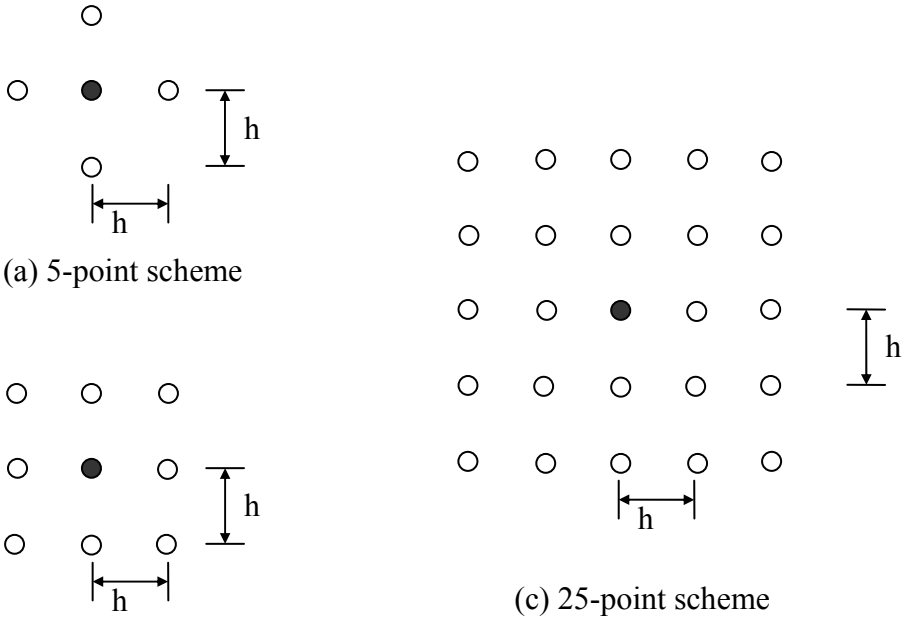

(a) 5-point scheme

(b) 9-point scheme

(c) 25-point scheme

Fig. 4. Cover schemes for 2D problem.

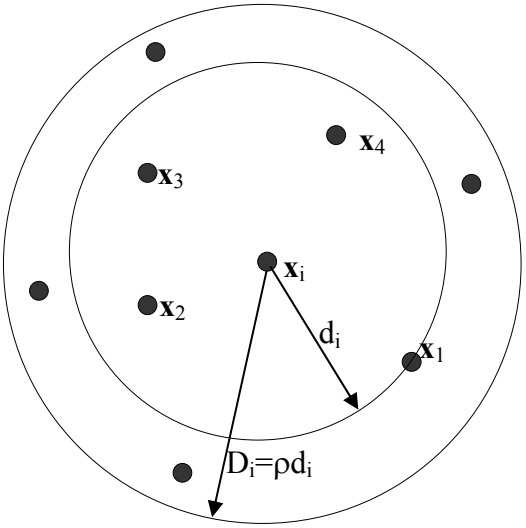

Fig. 6 A variable cover scheme.

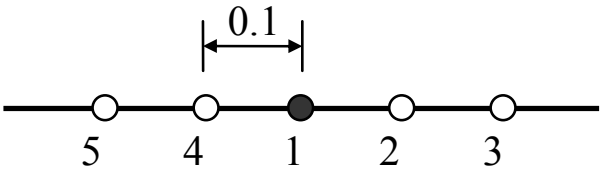

(a) Inter-nodal spacing and node numbering

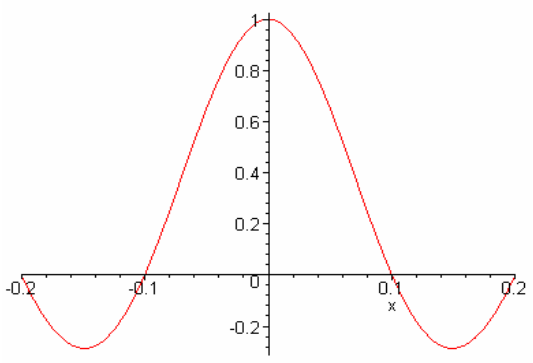

(b) $\psi_1^5(\mathbf{x})$

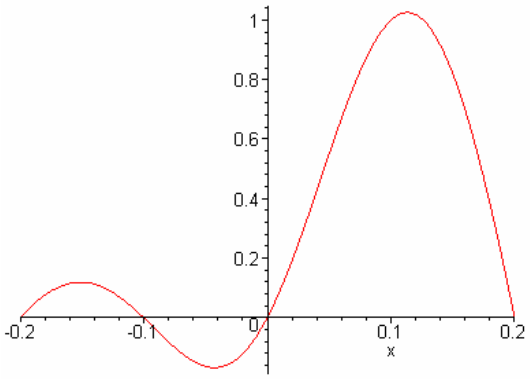

(c) $\psi_2^5(\mathbf{x}) = \psi_4^5(\mathbf{-x})$

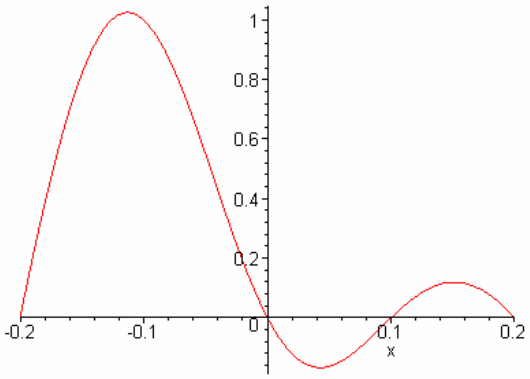

(e) $\psi_4^5(\mathbf{x}) = \psi_2^5(\mathbf{-x})$

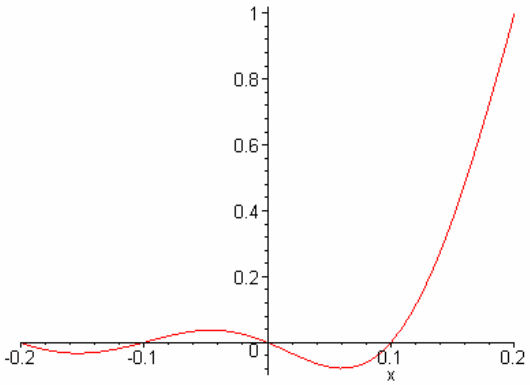

(d) $\psi_3^5(\mathbf{x}) = \psi_5^5(\mathbf{-x})$

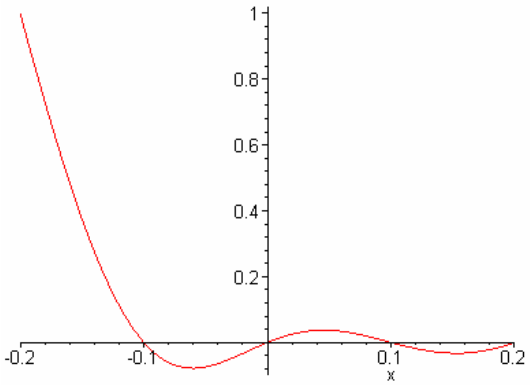

(e) $\psi_5^5(\mathbf{x}) = \psi_3^5(\mathbf{-x})$

Fig. 5. Shape functions for 1D LMQ approximation (h=0.1, c=0.2).

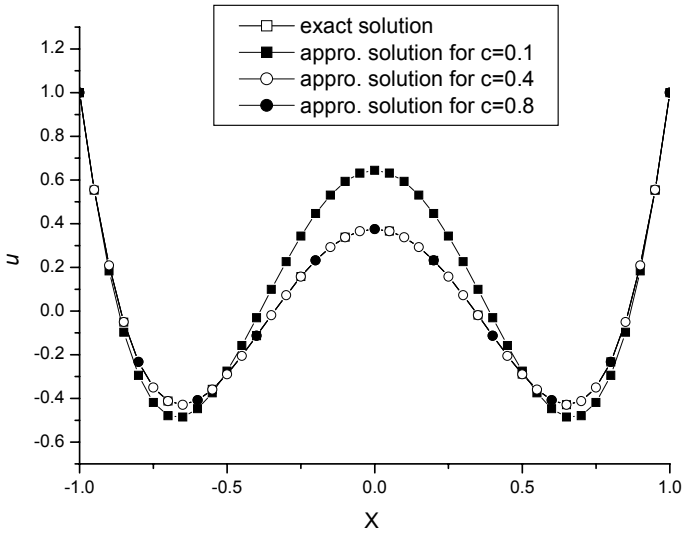

Fig. 7. Solutions of Example 1 (using h=0.05 and 5-point scheme).

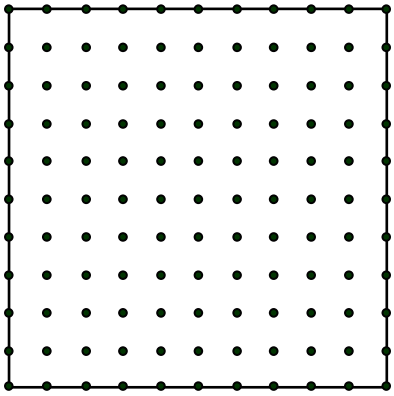

Fig. 8. Uniform nodal model (NR×NR) used in Examples 2 and 3 (e.g. NR=11).

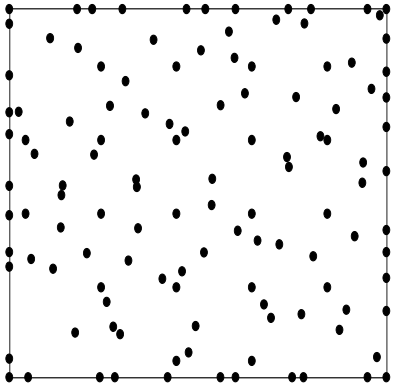

Fig. 9. Non-uniform nodal model used in Examples 2 and 3.

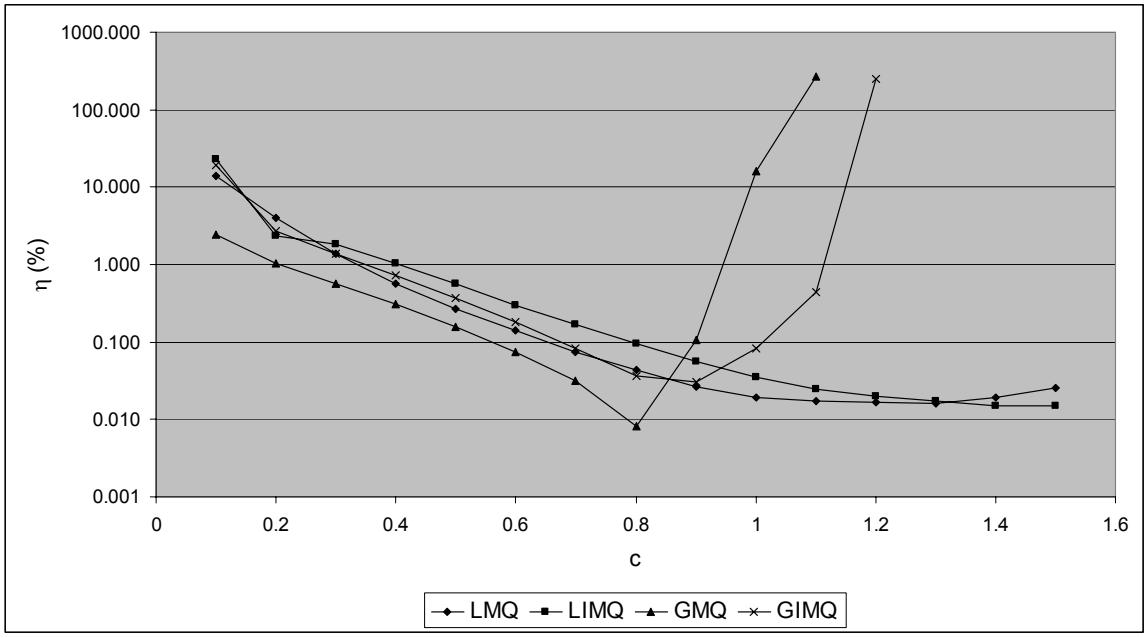

Fig. 10. Results of Example 2 by uniform nodal model and 25-point scheme.

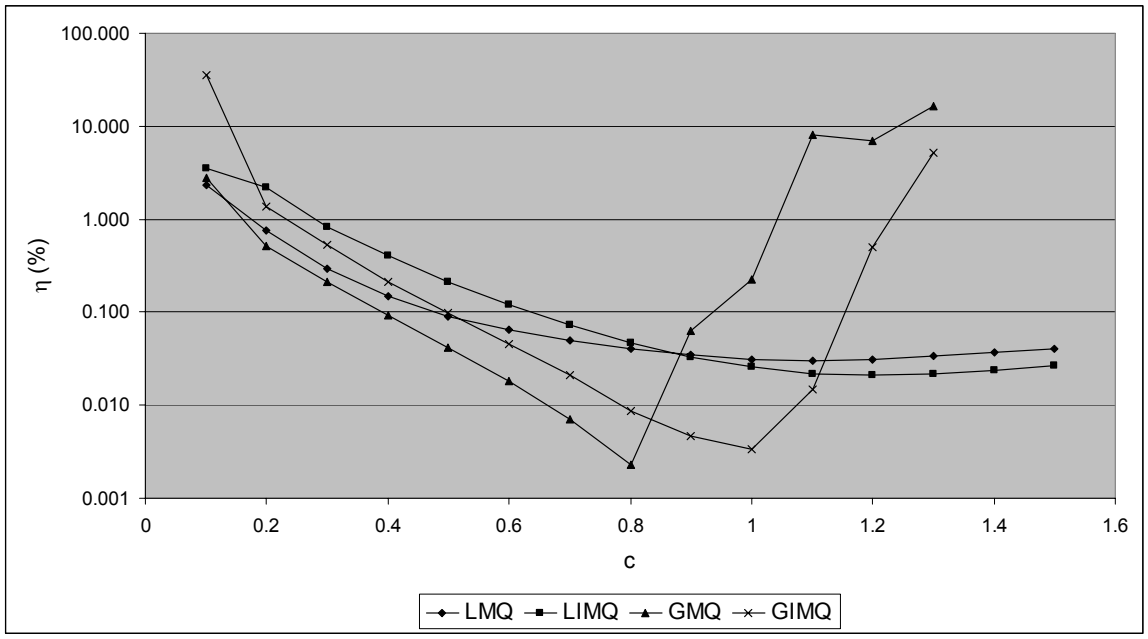

Fig. 11. Results of Example 2 by non-uniform nodal model and 25-point scheme.

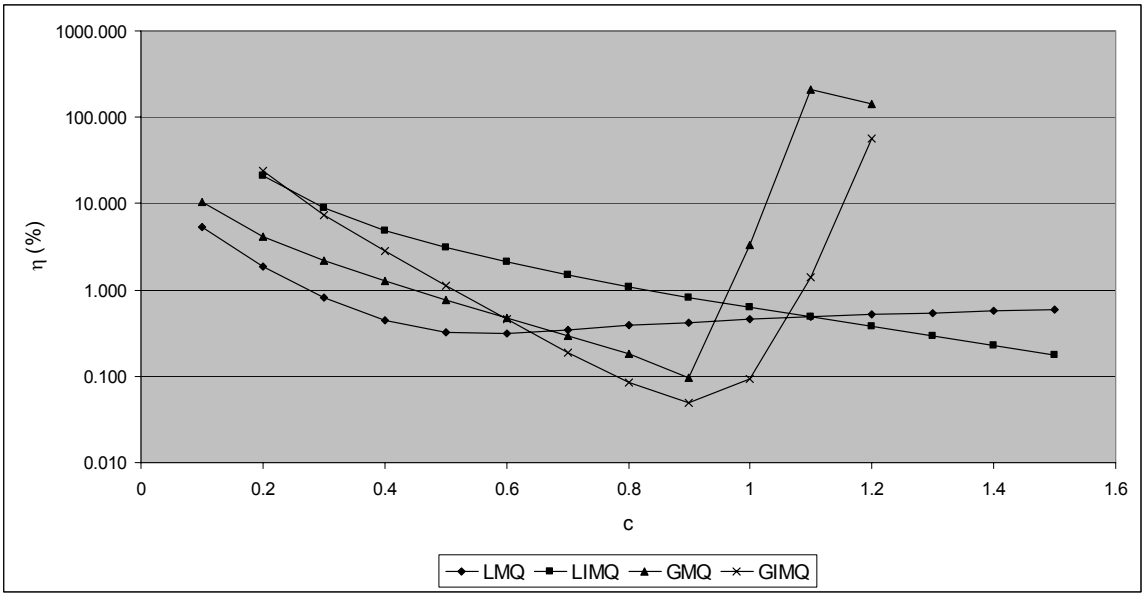

Fig. 12. Results of Example 3 by uniform nodal model and 25-point scheme.

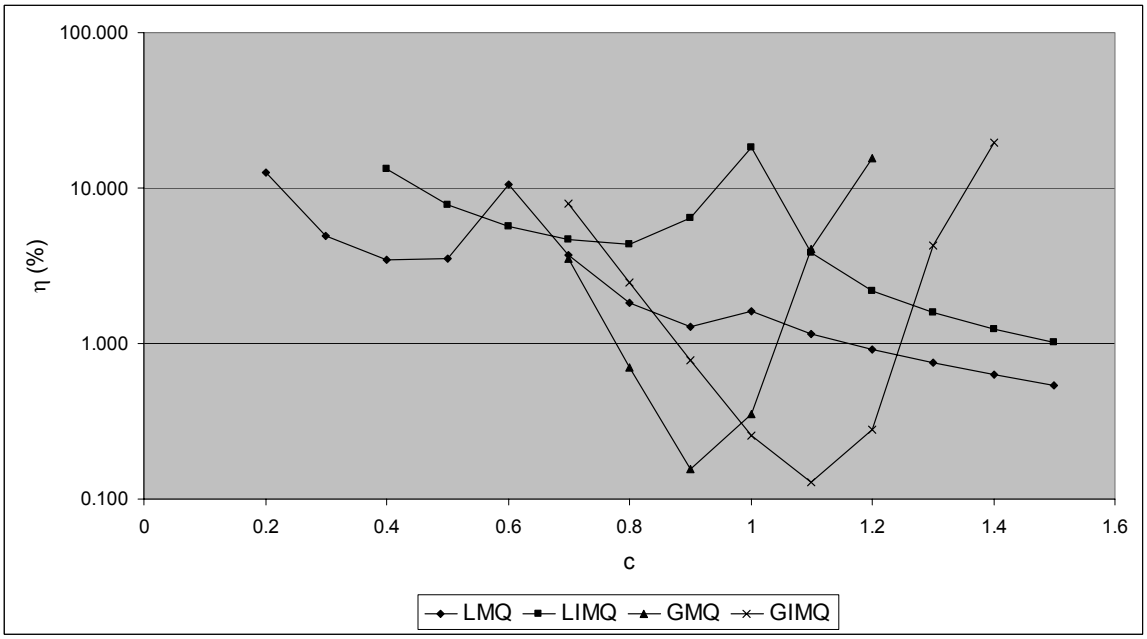

Fig. 13. Results of Example 3 by non-uniform nodal model and 25-point scheme.

Nodal spacing	3-point scheme (Fig. 3a)		5-point scheme (Fig. 3b)		7-point scheme (Fig. 3c)	
h	η(%)	R(η)	η(%)	R(η)	η(%)	R(η)
0.1	18.43	---	1.34	---	6.58	---
0.05	6.00	1.62	0.157	3.09	0.429	3.94
0.025	1.66	1.85	0.0145	3.44	0.0161	4.74

Table 1. Convergence rate of η in Example 1 for LMQ approximation with c=0.4

Nodal spacing	3-point scheme (Fig. 3a)		5-point scheme (Fig. 3b)		7-point scheme (Fig. 3c)	
h	η_x(%)	R(η_x)	η_x(%)	R(η_x)	η_x(%)	R(η_x)
0.1	19.97	---	8.76	---	7.77	---
0.05	7.24	1.46	1.73	2.34	0.892	3.12
0.025	2.52	1.52	0.31	2.48	0.0758	3.56

Table 2. Convergence rate of η_x in Example 1 for LMQ approximation with c=0.4

Free Parameter c	η(%)			
	LMQ	LIMQ	GMQ	GIMQ
0.1	13.7	23.1	2.456	19.2
0.2	4.064	2.335	1.034	2.670
0.3	1.386	1.813	0.575	1.380
0.4	0.572	1.048	0.309	0.723
0.5	0.270	0.561	0.157	0.367
0.6	0.139	0.302	0.0746	0.179
0.7	0.0755	0.166	0.0313	0.0832
0.8	0.0431	0.0943	0.0082	0.0367
0.9	0.0266	0.056	0.105	0.0305
1.0	0.0194	0.0349	15.9	0.0822
1.1	0.0171	0.025	265.6	0.443
1.2	0.0166	0.0199	>300	253.1
1.3	0.0161	0.0175	>300	>300
1.4	0.0192	0.0152	>300	>300
1.5	0.0258	0.0151	>300	>300

Table 3. Results of Example 2: relative errors of solution obtained by uniform nodal model and 25-point scheme with various values of c.

Free Parameter c	η(%)			
	LMQ	LIMQ	GMQ	GIMQ
0.1	2.334	3.56	2.786	35.9
0.2	0.751	2.167	0.521	1.371
0.3	0.294	0.825	0.214	0.535
0.4	0.149	0.401	0.092	0.210
0.5	0.091	0.215	0.042	0.097
0.6	0.064	0.122	0.018	0.046
0.7	0.050	0.073	0.00698	0.021
0.8	0.041	0.047	0.0023	0.0088
0.9	0.035	0.033	0.063	0.0047
1.0	0.031	0.026	0.228	0.0034
1.1	0.030	0.022	8.014	0.015
1.2	0.031	0.021	7.030	0.505
1.3	0.034	0.022	16.4	5.256
1.4	0.037	0.024	>20	>20
1.5	0.040	0.027	>20	>20

Table 4. Results of Example 2: relative errors of solution obtained by non-uniform nodal model and 25-point scheme with various values of c.

Nodal model N_RxN_R	Nodal spacing h	5-point scheme (Fig. 4a)		9-point scheme (Fig. 4b)		25-point scheme (Fig. 4c)	
		η(%)	R(η)	η(%)	R(η)	η(%)	R(η)
6×6	0.2	14.13	---	10.73	---	1.34	---
11×11	0.1	5.49	1.36	3.75	1.52	0.57	1.23
21×21	0.05	1.59	1.79	1.09	1.78	0.066	3.11

Table 5a. Convergence rate of η in Example 2 for LMQ approximation with c=0.4

Nodal model N_RxN_R	Nodal spacing h	5-point scheme (Fig. 4a)		9-point scheme (Fig. 4b)		25-point scheme (Fig. 4c)	
		η_x(%)	R(η_x)	η_x (%)	R(η_x)	η_x (%)	R(η_x)
6×6	0.2	19.85	---	15.64	---	12.09	---
11×11	0.1	6.08	1.71	4.14	1.92	2.65	2.19
21×21	0.05	1.52	2.00	0.96	2.11	0.47	2.50

Table 5b. Convergence rate of η_x in Example 2 for LMQ approximation with c=0.4

Nodal model N_RxN_R	Nodal spacing h	5-point scheme (Fig. 4a)		9-point scheme (Fig. 4b)		25-point scheme (Fig. 4c)	
		η(%)	R(η)	η(%)	R(η)	η(%)	R(η)
6×6	0.2	19.40	---	15.60	---	2.49	---
11×11	0.1	6.28	1.63	4.84	1.69	1.03	1.27
21×21	0.05	1.69	1.89	1.32	1.88	0.12	3.10

Table 6a. Convergence rate of η in Example 2 for LIMQ approximation with c=0.4

Nodal model N_RxN_R	Nodal spacing h	5-point scheme (Fig. 4a)		9-point scheme (Fig. 4b)		25-point scheme (Fig. 4c)	
		η_x(%)	R(η_x)	η_x (%)	R(η_x)	η_x (%)	R(η_x)
6×6	0.2	23.87	---	21.10	---	23.2	---
11×11	0.1	5.72	2.06	5.01	2.07	7.03	1.72
21×21	0.05	1.14	2.33	1.03	2.28	1.45	2.28

Table 6b. Convergence rate of η_x in Example 2 for LIMQ approximation with c=0.4

Free Parameter c	η(%)			
	LMQ	LIMQ	GMQ	GIMQ
0.1	5.318	>25	10.6	>25
0.2	1.844	21.3	4.169	23.8
0.3	0.814	8.873	2.174	7.405
0.4	0.443	4.938	1.264	2.829
0.5	0.319	3.104	0.768	1.135
0.6	0.313	2.100	0.476	0.458
0.7	0.346	1.493	0.298	0.187
0.8	0.386	1.098	0.184	0.0855
0.9	0.424	0.828	0.0976	0.0495
1.0	0.459	0.633	3.367	0.0928
1.1	0.490	0.489	212.7	1.383
1.2	0.520	0.379	143.5	56.2
1.3	0.547	0.294	>150	>100
1.4	0.575	0.227	>150	>100
1.5	0.602	0.175	>150	>100

Table 7. Results of Example 3: relative errors of solution obtained by uniform nodal model and 25-point scheme with various values of c.

Free Parameter c	η(%)			
	LMQ	LIMQ	GMQ	GIMQ
0.1	>15	>15	>30	>30
0.2	12.6	>15	>30	>30
0.3	4.910	>15	>30	>30
0.4	3.468	13.2	>30	>30
0.5	3.535	7.873	>30	>30
0.6	10.6	5.695	>30	25.5
0.7	3.683	4.653	3.527	7.997
0.8	1.828	4.373	0.7052	2.489
0.9	1.283	6.399	0.1545	0.7767
1.0	1.612	18.2	0.3492	0.2561
1.1	1.155	3.831	4.040	0.1291
1.2	0.9194	2.166	15.5	0.2782
1.3	0.7551	1.573	>20	4.307
1.4	0.6334	1.237	>20	19.5
1.5	0.5420	1.017	>20	>20

Table 8. Results of Example 3: relative errors of solution obtained by non-uniform nodal model and 25-point scheme with various values of c.

Nodal model N_RxN_R	Nodal spacing h	5-point scheme (Fig. 4a)		9-point scheme (Fig. 4b)		25-point scheme (Fig. 4c)	
		η(%)	R(η)	η(%)	R(η)	η(%)	R(η)
6×6	0.2	137.90	---	23.6	---	11.60	---
11×11	0.1	14.77	3.22	18.30	0.37	1.86	2.64
21×21	0.05	8.00	0.89	6.51	1.49	0.61	1.61

Table 9a. Convergence rate of η in Example 3 for LMQ approximation with c=0.2

Nodal model N_RxN_R	Nodal spacing h	5-point scheme (Fig. 4a)		9-point scheme (Fig. 4b)		25-point scheme (Fig. 4c)	
		η_x(%)	R(η_x)	η_x (%)	R(η_x)	η_x (%)	R(η_x)
6×6	0.2	196.75	---	30.72	---	29.23	---
11×11	0.1	20.71	3.25	48.20	0.65	7.25	2.01
21×21	0.05	6.52	1.67	6.42	2.91	0.77	3.24

Table 9b. Convergence rate of η_x in Example 3 for LMQ approximation with c=0.2